Broadband visual stimuli improve neuronal representation and sensory perception

Elisabeta Balla*[1,2,3], Christopher Wiesbrock*[1,3], Jenice Linde[1,3], Simon Musall[1,3,4], Björn M. Kampa[1,2,3]

[1] Systems Neurophysiology, Institute for Zoology, RWTH Aachen University, Aachen, Germany

[2] JARA BRAIN Institute of Neuroscience and Medicine (INM-10), Forschungszentrum Jülich, Jülich, Germany

[3] Research Training Group 2416 MultiSenses – MultiScales, RWTH Aachen University, Aachen, Germany

[4] Bioelectronics, Institute of Biological Information Processing-3, Forschungszentrum Jülich, Jülich, Germany

* denotes equal contribution

Abstract

Natural scenes are composed of complex distributions of visual features that drive neural response patterns and shape visual perception. However, most stimuli that are commonly used in vision research only reveal neural responses to single features, such as a specific stimulus orientation. How larger feature distributions affect neural responses and visual perception is therefore poorly understood. To address this question, we presented broadband visual stimuli with parametrically-controlled bandwidth of stimulus orientations and spatial frequencies to awake mice while recording the activity of neural populations in the primary visual cortex with two-photon imaging. Matching the orientation bandwidth of broadband stimuli to naturalistic images strongly increased neural responses and improved feature discrimination performance. Correspondingly, increasing orientation bandwidth also improved the performance of mice in a visual discrimination task. Our results strongly suggest that the visual system is tuned to the feature distributions of naturalistic visual inputs, with broader feature distributions driving more robust neural responses and enhanced visual perception.

Introduction

The identification of the position and structure of visual objects in the environment is among the main computations of the visual system. The accurate execution of this task critically relies on specific features of visual objects, such as their texture and relative size, which can be derived from the orientation and spatial frequency of incoming visual inputs. Receptive fields of neurons in the primary visual cortex (V1) are therefore sparse representations of the visual scenery[1–4], and selectively respond to prominent features, such as the orientation of elongated edges[5–8]. However, edge orientations in natural scenes are not statistically independent from each other but appear as specific combinations of common orientations, especially horizontal and vertical edges[9,10]. The visual system has therefore likely evolved to be well-tuned to the statistics of these features in the natural environment and shows highly variable and non-linear responses to complex visual stimuli[1,10–12]. In fact, even individual V1 neurons respond with high specificity to different natural images and exhibit complex tuning properties that go far beyond what could be inferred by their responses to simple sine-wave gratings or Gabor patches[12,13]. The conventional approach of studying the neural encoding of visual information by using a limited set of simple visual stimuli is therefore inadequate to identify the key properties of neural responses in the visual system. This approach only covers a very small range of the possible visual feature distributions, providing a limited view of complex visual processing. An alternative approach is to use natural scenes or images to identify neural response features to complex stimuli that match the statistics of the environment[14–16]. But since natural images are not

parametrically well-defined[17,18], very large sets of images and complex models are required to identify meaningful neural response features. Moreover, the presentation of large sets of images is often prohibited by the limited number of neural responses that can be obtained for each stimulus[12,13,19].

A powerful solution for this trade-off between well-controlled but overly simple gratings versus highly complex and unconstrained naturalistic stimuli are random phase textures, so-called motion clouds[20]. Motion clouds provide a parametrically well-defined visual stimulus that can closely approximate the feature distributions of naturalistic visual inputs. These stimuli allow for a tailored bandwidth assignment to capture specific distributions of visual features, such as edge orientations, that closely match those found in natural stimuli. Motion clouds therefore offer a controlled framework for studying the role of specific feature distributions in both physiological and behavioral experiments. However, so far motion clouds have not been widely tested in awake neural recordings and it remains largely unknown how changing the bandwidth of different visual features, such as edge orientations or spatial frequency, affects single-neuron responses and visual perception. Theoretical models suggest that broadband stimuli might activate more neurons with diverse tuning to visual features, but inhibitory feedback could also reduce their individual contributions to keep the overall network activity level constant[21–23]. This could also explain seemingly contradictory behavioral results in humans where increasing the bandwidth of spatiotemporal frequencies in motion clouds improves the coupling of oculomotor responses with visual motion but does not enhance speed perception[21].

To directly assess the impact of different feature bandwidths on neural activity, we presented motion cloud stimuli to awake mice and used two-photon imaging to measure the responses of individual V1 neurons to different bandwidths of orientations and spatial frequencies. We simultaneously imaged a large amount of V1 neurons in layer 2/3, exhibiting diverse visual tuning properties to visual gratings[24–28]. Increasing the orientation bandwidth of motion clouds activated more V1 neurons and also increased their neural response magnitude. In contrast, increasing spatial frequency bandwidth only weakly affected neural responses. We then trained mice to either discriminate the orientation or frequency of motion cloud stimuli. Consistent with our neural recordings, increasing frequency bandwidth had no impact on behavior while increasing orientation bandwidth improved perceptual performance. Our results demonstrate that neurons are tuned towards stimuli with a broad distribution of visual features instead of narrow gratings, suggesting that cortical processing and visual perception is optimized for visual stimuli that match the statistics of natural sensory inputs.

Results

Orientation bandwidth of visual stimuli recruits additional neuronal populations in mouse V1

Natural scenes contain edges with a broad range of orientations that can strongly vary in different spatial locations (Fig. 1a). To test if visual neurons are tuned to such specific orientation distributions (orientation bandwidth), we therefore designed different sets of motion cloud stimuli to match the different bandwidths found in naturalistic visual sceneries[10,29] (Fig. 1b). All motion clouds consisted of a spatial frequency of 0.04 cpd. and vertical orientation (0°), to match the response tuning of neurons in mouse V1 and higher visual areas[28,30,31], but were generated with different orientation bandwidths

(narrow-, mid-, and broad-range: 5°, 25°, 45°, respectively). We then presented motion clouds to awake, head-fixed mice while measuring the neuronal responses of layer 2/3 neurons in V1, expressing the calcium indicator GCaMP6f (Fig. 1c, d). To identify significantly responsive neurons, we then computed the area under the receiver-operating characteristic curve (AUC) for each neuron and stimulus. Interestingly, increasing the orientation bandwidth strongly increased the number of visually-responsive neurons in each session (narrow range (5°): 33 ± 4 neurons, mid range (25°): 41 ± 4 neurons, broad range (45°): 60 ± 6 neurons; mean ± s.e.m., n = 18 sessions in 9 mice), demonstrating that broader orientation bandwidth stimuli recruit a much broader range of orientation-tuned neurons (Fig. 1e).

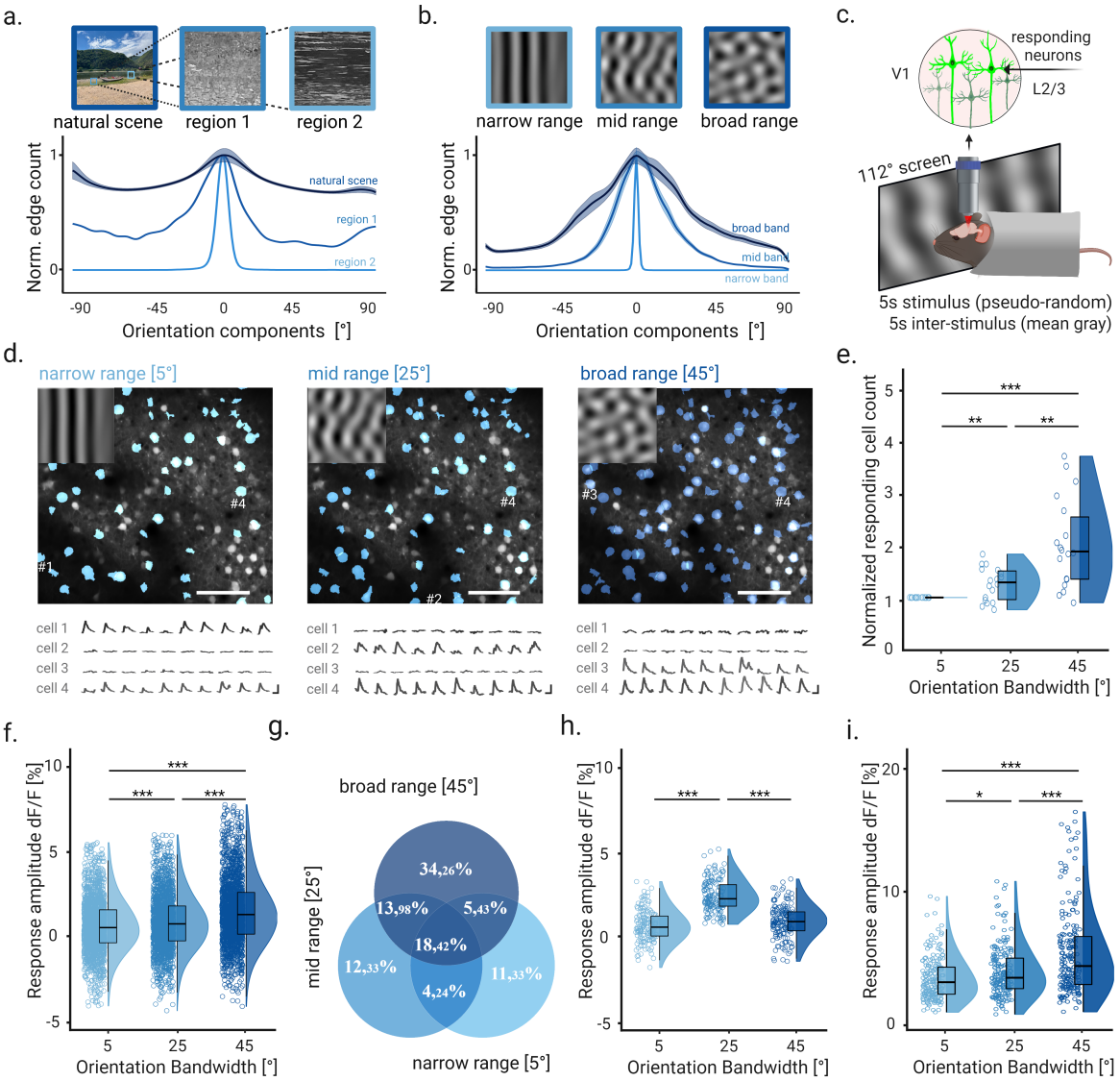

Figure 1. V1 neurons are most responsive to broad orientation bandwidths.

(**a**) Orientation distributions of selected scenes in an example natural image. (**b**) Orientation distributions of selected motion clouds with increasing orientation bandwidths (light to dark blue). (**c**) Schematic of the visual stimulation and imaging setup. Mice were head-fixed and shown a pseudo-random sequence of motion clouds with differing orientation bandwidths while imaging neural activity in layer 2/3. (**d**) Example two-photon imaging planes, showing V1 neurons from the same field of view that respond to different orientation bandwidths (5°, 25°, 45°, blue masks show responsive cells, scale bar 100µm). Corresponding stimuli are shown at the top left. Traces below show visual responses of 4 example cells with different orientation bandwidth tuning (scale bar 1s, 20% dF/F). (**e**) Counts of responsive neurons to a given orientation bandwidth, normalized by the number of cells re-

sponding to the narrow orientation bandwidth (5°) (n = 18 sessions). (**f**) Difference between mean response amplitude versus baseline for each orientation bandwidth. Shown are all neurons with a significant response for at least one stimulus (1509 responsive neurons out of 4892 neurons in total). (**g**) Distribution of neurons that significantly responded to a single or multiple orientation bandwidths. Shown are percentages for all responsive neurons. (**h**) Same as in panel f but only for neurons that selectively showed a positive response to the mid-range bandwidth (in total 186 neurons from all sessions). (**i**) Same as in panel f but only for neurons that consistently responded positively to all bandwidths (in total 278 neurons from all sessions). Stars in all panels show Bonferroni-corrected significance from a two-sided Wilcoxon signed rank test.

We then tested how changes in orientation bandwidth affect the magnitude of neural responses. Reflecting the overall increase in responding neurons, increasing orientation bandwidth also strongly increased the neural responses, which were the largest for the broadest orientation bandwidth (45°, Fig. 1f). Expanding the orientation bandwidth therefore increased both the number and magnitude of stimulus-responsive V1 neurons. To test if increased neural responsiveness to broader orientation bandwidth is caused by additional recruitment of neurons with specific, narrow orientation tuning[6], we then computed the number of V1 neurons that responded to each orientation bandwidth. Surprisingly, we found a high degree of specificity, with a sizable portion of neurons significantly responding to only a single orientation bandwidth or a specific combination of orientation bandwidths (Fig. 1g, see also example cells in 1d). Instead of an overall recruitment of neurons with narrow tuning, this suggests that V1 neurons exhibit a more complex orientation tuning that is selective for specific orientation bandwidths that match naturalistic stimulus patterns[32–35]. This also included a large fraction of neurons (186 neurons, 12.33% of all responsive cells) that responded most strongly to the mid-range orientation bandwidth, and therefore neither preferred the narrowest nor broad bandwidth stimuli (Fig. 1h). Lastly, we tested the response magnitude only for neurons that showed a significant response to all orientation bandwidths (center of the Venn diagram in Fig. 1g). These unselectively responding neurons also showed a clear increase in response magnitude with increasing orientation bandwidth (Fig. 1i), thus ruling out that larger responses were solely driven by subpopulation of V1 neurons that selectively responded to broad range stimuli. Instead, this general preference for broad orientation bandwidth might reflect a tuning bias of the visual system towards natural scenes which also contain broader average orientation bandwidth (Fig. 1a, dark blue trace).

Increasing spatial frequency bandwidth does not increase V1 responses

Similar to stimulus orientations, natural scenes also contain a large range of spatial frequencies that are not considered when using sinusoidal gratings with a fixed frequency. Spatial frequency distributions in naturalistic scenes follow a power law, with a higher power in the low-frequency bands for broad image features and weaker in the high-frequency bands for fine structural details[29,36] (Fig. 2a). V1 neurons are also well-tuned to spatial frequency[6,28,31], so we tested if enriching the frequency bandwidth of visual stimuli would affect neural responses similarly to orientation bandwidths. We therefore created motion cloud stimuli with different frequency bandwidths (0.004 cpd., 0.04 cpd. and 0.4 cpd.) with vertical orientation, matching the distributions found in different natural scenes (Fig. 2a, b). Visual stimuli were presented pseudo-randomly while measuring the activity of the same V1 neurons described above (Fig. 2c).

In contrast to our earlier results, increasing the frequency bandwidth did not significantly change the number of responsive neurons in each session (0.004 cpd.: 21 ± 4 neurons, 0.04 cpd.: 20 ± 5 neurons, 0.4 cpd.: 22 ± 4 neurons; mean ± s.e.m., n = 16 sessions in 9 mice) (Fig. 2d, e). Correspondingly, when comparing the response magnitude for all responsive neurons we found no significant differences across different bandwidths (Fig. 2f). A potential reason for this clear difference between orientation and spatial frequency bandwidth could be that V1 neurons already exhibit broad spatial frequency tuning, resulting in overlapping activation of these neurons by different spatial frequency bandwidths[28].

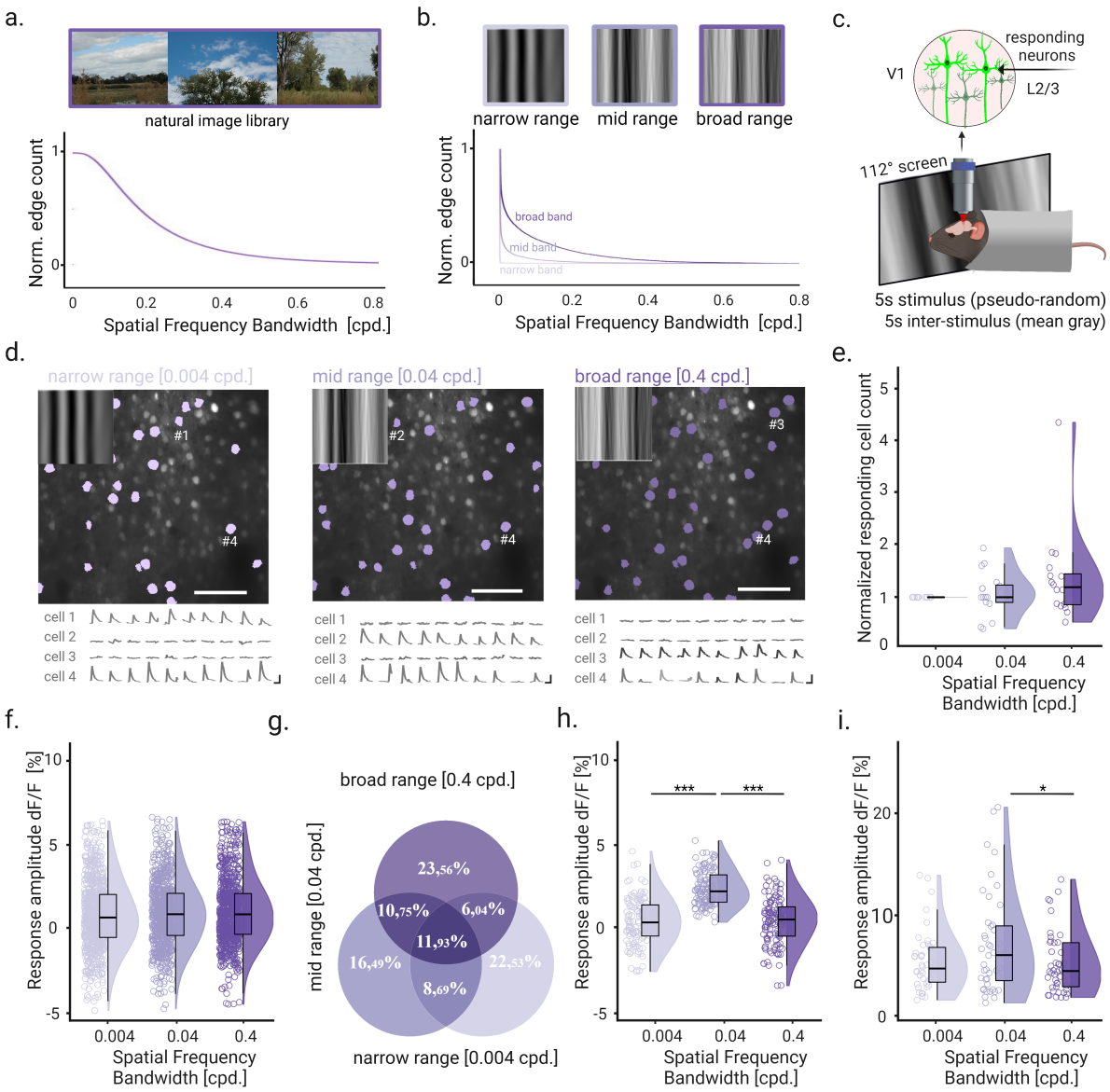

Figure 2. V1 neurons are selective but equally responsive to different frequency bandwidths. (**a**) Spatial frequency distributions of different example natural images. (**b**) Spatial frequency distributions of selected motion clouds with increasing frequency bandwidths (light to dark blue). (**c**) Schematic of the visual stimulation with motion clouds of different spatial frequency. (**d**) Example two-photon imaging planes, showing V1 neurons from the same field of view that respond to different frequency bandwidths (0.004 cpd., 0.04 cpd., 0.4 cpd., blue masks show responsive cells, scale bar 100 µm). Corresponding stimuli are shown at the top left. Traces below show visual responses of 4 example cells with different frequency bandwidth tuning (scale bar 1s, 20% dF/F). (**e**) Counts of responsive neurons to a given frequency bandwidth, normalized by the number of cells responding to the narrow frequency bandwidth (0.004 cpd.). (n = 16 sessions). (**f**) Difference between mean re-

sponse amplitude versus baseline for each frequency bandwidth. Shown are all neurons with a significant response for at least one stimulus (679 responsive neurons out of 3185 neurons in total). (**g**) Distribution of neurons that significantly responded to a single or multiple frequency bandwidths. Shown are percentages for all responsive neurons. (**h**) Same as in panel f but only for neurons that selectively responded to the mid-range bandwidth (in total 112 neurons from all sessions). (**i**) Same as in panel f but only for neurons that consistently responded to all bandwidths (in total 81 neurons from all sessions). Stars in all panels show Bonferroni-corrected significance from a two-sided Wilcoxon signed rank test.

To test this hypothesis, we computed the number of neurons that significantly responded to a specific spatial frequency bandwidth. As with orientation bandwidth, we found a high degree of specificity, with a roughly equal quantity of neurons responding to different frequency bandwidths or bandwidth combinations (Fig. 2g, example cells in 2d). The lack of increased responsiveness to broader frequency bandwidths was therefore not because of very broad frequency tuning of V1 neurons that may have caused a large overlap in neural responses to different frequency bandwidths. Instead, we again observed selective tuning to different frequency bandwidths, including prominent responses to the mid-range frequency bandwidth in a sizable portion of neurons (Fig. 2h). Lastly, the response magnitude for unselectively responding neurons did also not increase for larger frequency bandwidths. Instead, there was even a slight decrease in response magnitude between mid and broad range frequency bandwidths (Fig. 2i). Together, these results demonstrate that V1 responses are well-tuned to specific spatial frequency bandwidths.

To further test if the specificity of neural responses clearly differs for the range of orientations and spatial frequencies that we used in our motion cloud stimuli, we also presented simple gratings with different combinations of orientation and spatial frequency (Supplementary Fig. S1). While we observed diverse neural tuning to the presented gratings, the average tuning width of the responding neurons was similar for the range of tested orientations and spatial frequencies. This further argues against the hypothesis that the lack of increased neural responses to broadband spatial frequency stimuli was because of particularly broad spatial frequency tuning that prevented further recruitment of specific subpopulations. Instead, stronger responsiveness to broader orientation bandwidth appears to be a specific feature of V1 neurons that does not generalize to spatial frequency.

Neural discrimination performance is enhanced by broader orientation bandwidth

We next wondered if increasing motion cloud bandwidth also improves the neural representation of sensory information, thus making broadband stimuli more perceptually distinct from each other. To test this hypothesis, we presented stimuli with a different central orientation (0° or 90°) or central spatial frequency (0.04 cpd. or 0.16 cpd.) and measured the impact of motion cloud bandwidth on the ability of neurons to discriminate between these differences (Fig. 3a, e; Supplementary Fig. S2, S3). To avoid ambiguity, we did not change the bandwidth of stimulus orientations or spatial frequency together but instead compared neural responses to the central feature while changing the bandwidth of the other. Similar to our previous results, increasing the orientation bandwidth with a central spatial frequency of 0.16 cpd. also strongly increased the number and magnitude of responsive neurons (narrow (5°): 40 ± 4 neurons, mid (25°): 41 ± 3 neurons, broad (45°): 52 ± 5 neurons; mean ± s.e.m., n = 18 sessions in 9 mice; Fig. 3b, c; Supplementary Figure S2). Larger neural responses to broader orientation bandwidth are therefore not limited to a specific central spatial frequency and broadband

stimuli might enhance the discriminability of different spatial frequencies by driving stronger responses in a larger population of V1 neurons. Conversely, broadband stimulation may also have the opposite effect by driving the same strong responses in the same neurons, regardless of the central spatial frequency. For each neuron, we therefore computed the absolute AUC between responses to different spatial frequencies with either narrow or broad orientation bandwidth (Fig. 3d). The discriminability between spatial frequencies was strongly enhanced with broader orientation bandwidth ($AUC_{5°}$ = 0.29 ± 0.005, $AUC_{45°}$ = 0.35 ± 0.005; mean ± s.e.m., n = 2202 neurons), demonstrating that broadband motion clouds are more effective in representing specific sensory information. In contrast, broadening spatial frequency bandwidth did not increase the number or magnitude of neural responses with a central orientation of either 0° or 90° (Fig. 3f, g; Supplementary Fig. S3). Consequently, we found no significant difference in orientation discriminability for either narrow or broad frequency bandwidth ($AUC_{0.004cpd.}$ = 0.29 ± 0.007, $AUC_{0.4cpd.}$ = 0.30 ± 0.008; mean ± s.e.m., n = 985 neurons, Fig. 3h). These results demonstrate that naturalistic broadband stimuli not only increase the overall strength but also the discriminability of visual responses which might result in enhanced perceptual accuracy

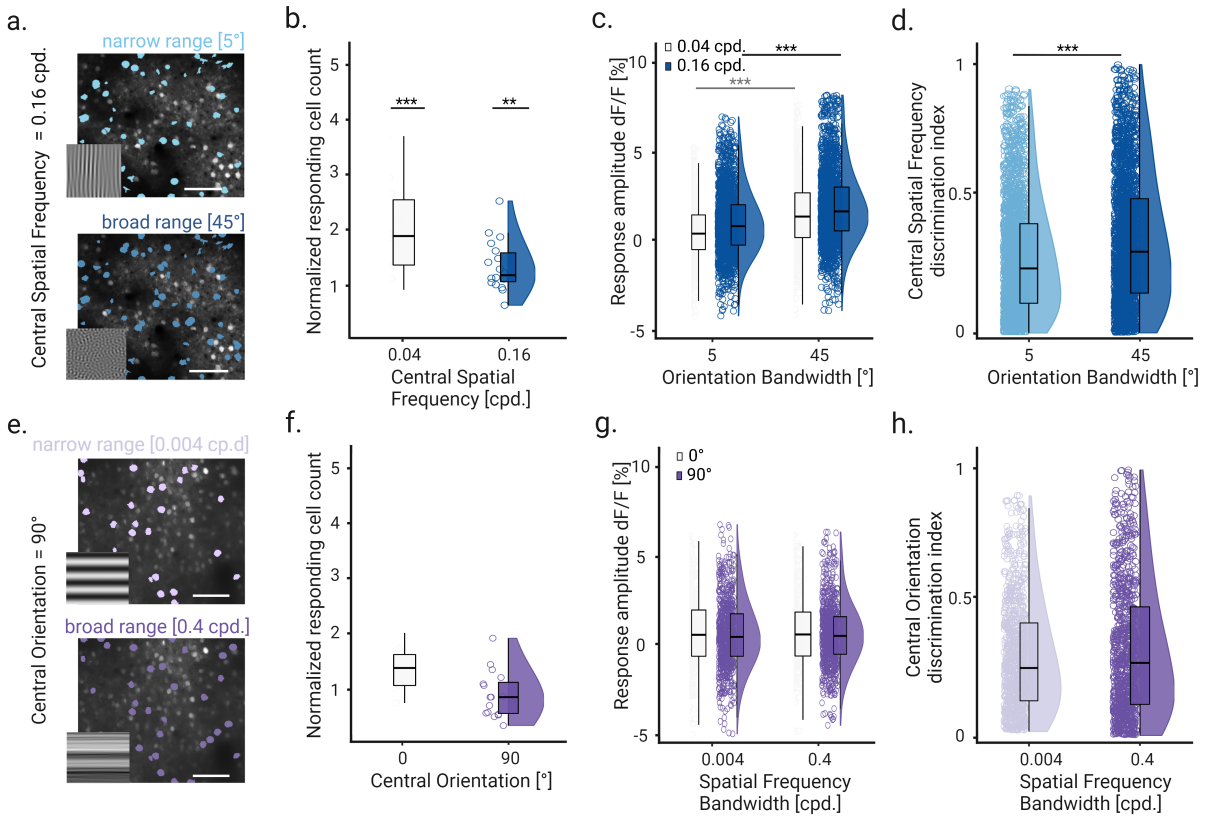

Figure 3. Increasing orientation bandwidth improves stimulus discriminability in V1 neurons
(**a**) Example field of view of an experiment with the central spatial frequency of 0.16 cpd. and narrow or broad orientation bandwidth. Clearly visible are increased cell numbers with broad orientation bandwidth. Stimulus illustrated at the bottom left of the plane, scale bar 100µm. (**b**) Number of responsive cells to broad orientation bandwidth (45°) with either 0.04 cpd. or 0.16 cpd. spatial frequency, normalized by the respective number of cells responding to the lowest orientation bandwidth (5°). Data for 0.04 cpd. are the same as in Figure 1 and shown here for reference as a box plot. Stars show Bonferroni corrected significance for one-sided Wilcoxon rank sum test against 1 (n = 18 sessions). (**c**) Mean response amplitude for all responsive neurons to each orientation bandwidth and central 0.16 cpd. spatial frequency. (Blue raincloud plots, n = 2202 responsive neurons). Boxplot shows responses to 0.04 cpd. for comparison (same as in Fig. 1g). (**d**) Discriminability between neural responses

to 0.04 cpd. or 0.16 cpd. Central spatial frequency for narrow and broad orientation bandwidth. (n = 2202 neurons.) Stars in panels c and d show Bonferroni-corrected significance from two-sided Wilcoxon signed rank test. (**e**) Example field of view of an experiment with 90° central orientation and narrow or broad frequency bandwidth. Increasing frequency bandwidth did not increase the number of responsive neurons and response patterns were largely similar across different stimuli. (**f-i**) Same as panels **(b-d)** but for narrow and broad frequency bandwidth and 0° and 90° central orientation.

Spatial frequency perception is enhanced by broader orientation bandwidth

Our results show that neural responses in V1 are enhanced when increasing orientation bandwidth, which also increased the neuronal discriminability of these broadband visual stimuli. To assess if increased neuronal discriminability also results in enhanced visual perception, we trained mice to perform a visual discrimination task in a custom-build touchscreen chamber[37] (Fig. 4a). Here, mice had to discriminate between motion clouds by touching one of the two presented stimuli on a touch-sensitive screen and were rewarded when choosing the target stimulus. For two groups of mice (6 mice each), motion clouds either differed in their central spatial frequency (0.04 cpd. target versus 0.16 cpd. non-target; Fig. 4b, left) or central orientation (0° target versus 90° non-target; Fig. 4b, right). In addition, we again varied the orientation or frequency bandwidth of the presented motion clouds, to test their impact on discrimination performance. As in our earlier experiments, the bandwidth was only altered for the stimulus parameter that was not tested in the discrimination task to avoid any ambiguity. In the orientation discrimination task, we thus varied spatial frequency bandwidth while varying orientation bandwidth during spatial frequency discrimination (Fig. 4b).

Animals in both groups reliably learned to perform either the orientation or spatial frequency discrimination task and achieved comparable expert performance above 80% correct trials (Fig. 4c). Increasing the orientation bandwidth also improved spatial frequency discrimination performance (narrow (5°): 77.02 ± 0.02% correct, mid range (25°): 77.63 ± 0.02% correct, broad (45°): 82.78 ± 0.01% correct, mean ± s.e.m., n = 46 sessions), demonstrating that broad orientation bandwidth not only improved neural response discriminability but directly enhanced spatial frequency perception. Conversely, increasing spatial frequency bandwidth did not further improve orientation discrimination performance and even showed a trend towards reduced performance with higher frequency bandwidth (Fig. 4d).

These findings clearly show that the observed changes in V1 responses translate into corresponding changes in visual perception, with the greatest discrimination performance observed for broad orientation bandwidths. A possible reason for the unchanged discrimination performance across spatial frequency bandwidths could be that perceptual changes are only visible near the frequency discrimination threshold, where even small perceptual variations can effectively impact behavior. We therefore further tested different spatial frequency bandwidths over a larger range of orientation differences. Using a staircase procedure, we dynamically changed the orientation difference between target and non-target stimuli to identify the orientation discrimination threshold for each mouse across individual sessions. However, the obtained discrimination thresholds and psychometric curves were largely similar across frequency bandwidths (Fig. 4e, f) (45.7 degrees ± 2.34, 43.93 degrees ± 3.12, 49.34 degrees ± 2.46, mean ± s.e.m., at 72.7% orientation discrimination threshold for 0.004, 0.04,

and 0.4 cpd. frequency bandwidth, respectively, n = 18, 23 and 30 sessions), thus arguing against a notable impact of spatial frequency bandwidth on orientation perception.

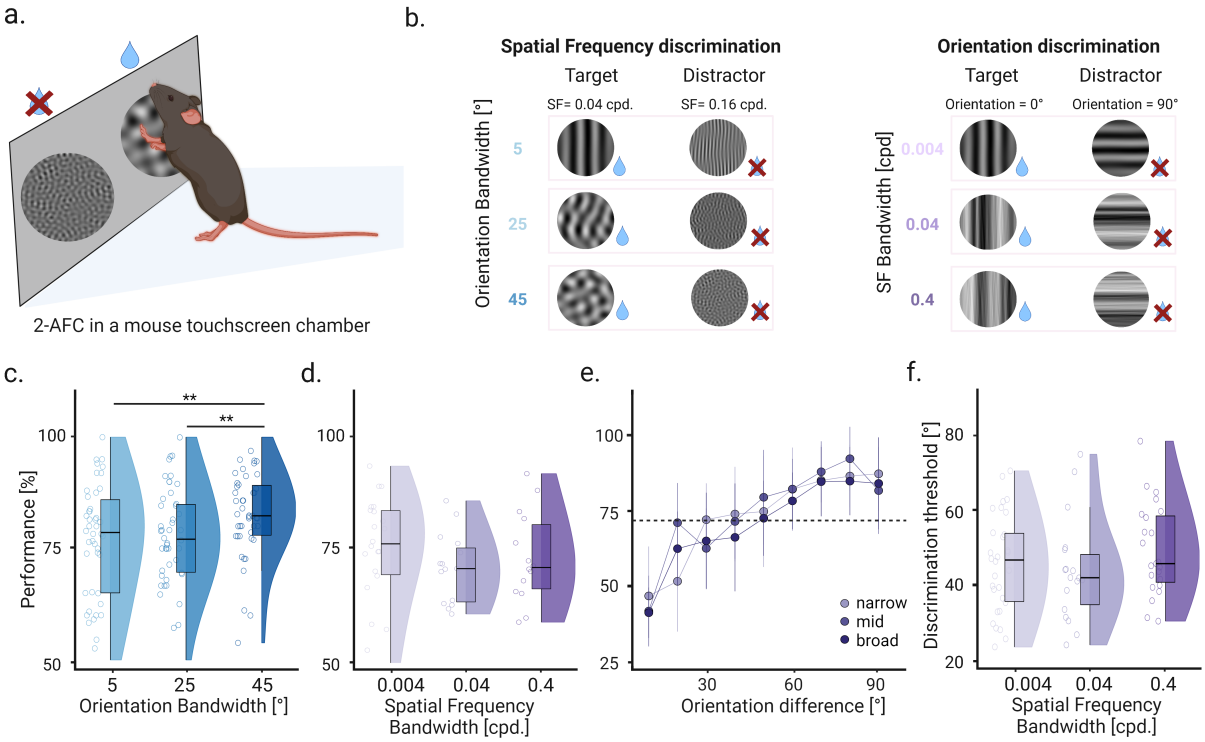

Figure 4. Increasing orientation bandwidth improves visual perception.
(**a**) Illustration of the visual discrimination task. Mice in a touchscreen chamber select target stimuli to obtain a reward. (**b**) Example stimuli for the spatial frequency discrimination task with different orientation bandwidths (left) and the orientation discrimination task with different spatial frequency bandwidths (right). (**c**) Spatial frequency discrimination performance for different orientation bandwidths. Spatial frequency discrimination performance was significantly higher for a larger orientation bandwidth. (n = 46 sessions.) (**d**) Same as **c** for the orientation discrimination with different spatial frequency bandwidths. (n = 17-25 sessions.) (**e**) Psychometric curves for orientation discrimination performance at different target-distractor orientation differences. Colors show curves for different spatial frequency bandwidths. Increasing spatial frequency bandwidth did not affect maximal performance or discrimination thresholds. The dashed line shows the 72.5% discrimination threshold. (Error bars show standard deviation over 18-30 sessions.) Stars in all panels show Bonferroni-corrected significance from two-sided Wilcoxon signed rank test. (**f**) Discrimination thresholds for the three spatial frequency bands show no significant differences. (n = 18-30 sessions.)

Discussion

Natural scenes are composed of broad distributions of edge orientations and spatial frequencies. To test how changes in the bandwidth of these visual features affect neural responses and visual perception we used motion cloud stimuli[20]. Presenting motion clouds with comparable broadband features as in natural scenes revealed clear tuning of V1 neurons to specific orientation and spatial frequency bandwidths in awake mice. Moreover, increasing orientation bandwidth also leads to stronger V1 responses, reflected in more responsive neurons and larger response amplitudes. This prominent increase in response strength could be an adaptive mechanism of the visual system to enhance the perception of specific broadband stimuli. Indeed, increasing the orientation bandwidth of visual stimuli also improved the discriminability of neural responses to motion clouds with different central spatial frequencies. Lastly, mice were more accurate in discriminating visual stimuli with broad compared to narrow orientation bandwidth, confirming an enhancement in visual perception.

Together, these results clearly demonstrate that V1 neurons are tuned to specific bandwidths of visual features, with broadband stimuli increasing neural response strength, stimulus discriminability, and visual perception.

We found more responding neurons in V1 upon visual stimulus enrichment, which correspondingly led to improved visual perception. This appears to be in contrast to a previous study in humans, showing that increasing the spatiotemporal frequency bandwidth of motion cloud stimuli does not improve speed perception[21]. A potential reason for this distinction could be that spatial and temporal frequency directly affect speed estimates[38–40], thus creating a complex inter-dependency between the enriched visual features and the tested perceptual feature. To avoid this confounding inter-dependency, we separated the enriched visual feature from the perceptual feature, by either increasing orientation bandwidth during spatial frequency discrimination or vice versa. Importantly, this allowed us to isolate the perceptual impact of each visual feature and reveal that only orientation but not spatial frequency bandwidth enrichment increased neural responses and sensory perception. Indeed, the lack of perceptual improvements with spatial frequency enrichment is in line with earlier results in humans[21] and strongly suggests that the perceptual effects of rich visual stimuli are selective for specific visual features, such as orientation bandwidth.

The reason for the selective increase in neural responses to broadband orientation, but not spatial frequency stimuli is unclear. An intuitive explanation is that broader neural tuning to spatial frequencies compared to orientations[28,30,31] might result in an unselective activation of broadly-responding neurons with different spatial frequency bandwidths. However, when we directly compared the tuning of V1 neurons to the same range of orientations and spatial frequencies that we used in our motion cloud stimuli, the tuning width of individual neurons was largely similar for both features (Supplementary Fig. S1). We also observed an equal amount of response specificity for different spatial frequency and orientation bandwidths (Fig. 1g, 2g), further suggesting that differences in neural tuning cannot explain the response preference to broadband orientation stimuli. Instead, increased neural responses to broadband orientations appear to be a specific feature of the visual cortex and could be an adaption to the orientation distributions in natural scenes (Fig. 1a).

A potential mechanism that could promote increased responses to broadband orientation stimuli are feedback projections from higher visual areas[41–44]. Top-down feedback is crucial for the integration of contextual cues beyond the receptive field of V1 neurons and attenuates neural responses to a visual stimulus when it is surrounded by a similar stimulus[42,45,46]. Such center-surround suppression emphasizes the differences between a visual stimulus and its background[47] and might represent a predictive coding mechanism in which top-down feedback conveys a prediction of incoming visual inputs that is subtracted from V1 responses[48–50]. Since the spatial consistency of the stimulus and background is much lower when increasing orientation versus spatial frequency bandwidth, this could result in reduced stimulus predictability of broadband orientation stimuli and in turn reduce surround suppression. Interestingly, broadband orientation stimuli also improved sensory perception, arguing that such a lack of stimulus predictability can improve the representation of visual input features.

Superposition of different oriented gratings has been shown to suppress cortical responses in cat[51–54]. However, facilitated responses have also been reported in monkey and mouse[32–35,55–57]. In fact, our results are in line with earlier observations that broadband visual stimuli are effective in activating mouse cortical neurons[6,58]. The large variety in cortical responses to multiple superimposed gratings could also be explained by orientation-specific horizontal interactions within V1[32,33] or by a thalamocortical feedforward mechanism[35]. Both mechanisms would also explain the particular tuning of V1 neurons to specific orientation and spatial frequency bandwidths that we observed in our study.

Earlier work also suggested that a lack of perceptual enhancement for enriched visual stimuli could be due to cortical gain normalization where increased sensory inputs are counter-balanced by divisive local inhibition[21–23]. Such gain normalization would predict that an increasing number of responsive neurons should be accompanied by increased local inhibition which reduces the magnitude of neural responses and maintains an equal level of overall response strength across different stimuli[42,52,59]. In contrast, we found that broadband orientation stimuli not only increased the number of responding neurons but also their response amplitudes (Fig. 1f). This was also the case for the selected neurons that responded to all motion clouds irrespective of their orientation bandwidth, ruling out the possibility that stronger responses were due to a bandwidth-specific sub-population of V1 neurons. Our results therefore argue against cortical gain normalization as a limiting factor for perceptual effects of rich visual stimuli.

Natural vision is broadband vision and simple gratings of a single orientation and spatial frequency are rarely present in a natural environment. The visual system is tuned to the statistics of natural inputs[1,10], which is represented in the ability of mice and humans to discriminate fine differences in visual features that are most common in the environment[10,28,37]. Natural scenes also consist of distributions of largely overlapping orientations around areas of interest[9] (see also Fig. 1a), leading to complex receptive fields of cortical neurons that respond more strongly to visual features when they are embedded in natural scenes instead of random or artificial backgrounds[8]. Revealing the computational principles of natural scene processing is therefore crucial in order to understand visual processing at large. Our results with broadband orientation motion clouds demonstrate that rich but parametrically-controlled visual stimuli are a promising tool to achieve this goal and reveal how the visual cortex has evolved to perceive our natural environment.

Methods

Surgical procedures. Six male and three female C57BL/6J mice aged (16-30) weeks were used for the imaging experiments and twelve male C57BL/6J mice from 8 weeks of age were used for the 2AFC tasks. All mice were kept on a reverse light cycle (light/dark cycle: 12/12 hours). Experiments were carried out according to the German animal protection law and local Ethics committee. Mice were anaesthetized using (1%-2.5%) isoflurane in oxygen and placed in a stereotaxic frame with stabilized and monitored body temperature (37°C). Eye ointment (Bepanthen, Bayer Vital GMBH) was placed on the ipsilateral eye and ophthalmic gel in the contralateral to keep them moisturized but also allow intrinsic imaging to follow. V1 location was confirmed with intrinsic imaging[28,30]. Following a medial incision, the skin was pushed aside and the skull around coordinate-based V1 position (3.5 mm posterior and 2.5 mm lateral from bregma) was carefully thinned. The anaesthetized mouse was then shown moving full field gratings in different orientations on the contralateral side to the imaged cortex. After functionally confirming the V1 location, a 4-mm-wide circular craniotomy was performed over the center of V1. A viral vector (AAV9.Syn.GCaMP6f.WPRE.SV40; Addgene, 1:10 dilution with PBS and mannitol) was then injected through a thin glass pipette with a micropump (UMP-3, World Precision Instruments). After injection, a 4-mm-wide round cover slip was placed inside the window and fixed with dental cement (DE Flowable composite). A metal head-holder was positioned attached with dental cement to allow subsequent head-fixation and imaging in the two-photon microscope setup.

Two-photon imaging. Two-Photon imaging was done in a custom-made setup with a resonant-scanning two-photon microscope (CRS 8KHz, Cambridge Technology) and a femtosecond-pulsed TI: Sapphire laser (Mai Tai Deep See, Spectra-Physics) tuned to 920 nm. Data acquisition and controls were performed the MATLAB-based Scanimage package[60]. Settings and laser power were kept constant across all mice and experiments. References from the vessel image, intrinsic imaging and injection site referencing were used to define the center of the primary visual cortex. Recordings were made from layer 2/3 of the primary visual cortex at a depth of 250-300 µm below the pial surface and 30 Hz frame rate at a pixel resolution of 512x512 pixels. Calcium traces were imaged from all neurons expressing GCamP6f under the synapsin promotor, which could be detected in the field of view.

Visual stimulation. Motion cloud stimuli were generated using the Motion Cloud Package[20], and adapted for display via custom written MATLAB scripts (MATLAB R2019b, MathWorks). The package follows a linear generative model for creating dense mixing of localized moving gratings with random positions based on predefined parameters. To ensure that neural responses were not strongly drive by the individual properties of these random phase motion textures, 10 realizations of 150 frames each were generated for each parameter combination. 20 repetitions of each stimulus when then presented for a duration of 5s in a pseudorandom sequence which avoided consecutive display of the same stimulus. Parameter combination and protocols are shown in Table 1. All motion clouds were created with a temporal frequency of 1 Hz, with 5 s stimulus duration and 5 s inter-stimulus interval during which a gray screen was shown. Stimuli were presented at 18 cm distance from the right eye on a gamma-corrected LED-backlit LCD monitor (BenQ XL2420T) placed at a 90° angle.

	Central ORIENTATION [°]		Orientation Bandwidth [°]			Central Spatial Frequency [cpd]		Spatial Frequency Bandwidth [cpd]		
Orientation Band enrichment	0		5	25	45	0.04	0.16	0.004		
Spatial frequency Band enrichment	0	90	3			0.04		0.004	0.04	0.4

397 **Table1. Specific Parameters per each protocol.** For the protocol used to investigate the effect of the
398 orientation bandwidth enrichment (orientation protocol, top row), the central orientation (first column) and spatial
399 frequency bandwidth (last column) were kept constant (respectively 0° and 0.04cpd.), but combinations of
400 orientation bandwidth (second column: 5°, 25°, 45°) and central spatial frequency (third column: 0.04 cpd. and
401 0.16 cpd.) were used. This amounted to a total of 6 different stimuli. The same principles were followed for the
402 protocol to investigate the effects of spatial frequency bandwidth enrichment (spatial frequency protocol, bottom
403 row).

404 **Touchscreen chamber experiments.** Behavioral experiments were performed in a custom-build operant
405 conditioning touchscreen chamber for automatized and standardized animal training[37]. All animals performed the
406 experiments under a water restriction regime and received at least 1.5 ml of water per day to maintain their
407 general well-being. They received water *ad libitum* on the weekends and had access to food *ad libitum*
408 throughout the experiment. All mice were daily weighted and monitored prior and during the behavioral
409 experiments. In the first phases of pre-training, the animals were habituated to the touchscreen chamber and
410 learned to associate a green light with the availability of a reward. After the animals were able to collect at least
411 one reward per minute, they proceeded to the next phase where they had to first touch the screen to receive a
412 reward, which was still indicated by a green light. Again, after the animals performed the sequence of touching
413 the screen and collecting a reward at least once a minute, they were moved to more specific trainings according
414 to orientation or spatial frequency discrimination. The *orientation discrimination task* was started with the training
415 for an easy discrimination, where the animals had to discriminate a horizontal (target) from a vertical (distractor)
416 sine-wave grating with a spatial frequency of 0.04 cpd. After the animals reached a performance of 80% correct
417 responses, we proceeded with a staircase procedure. In this staircase procedure, the difficulty level was
418 dynamic. Every correct response was followed by a decrease in orientation difference of 3°, while an incorrect
419 response was followed by an increase in orientation difference of 8°, which led to a target performance of 72,7%.
420 After the animals were able to perform in the staircase procedure, it was possible to obtain one orientation
421 discrimination threshold per session. In randomized sessions, different motion clouds with different spatial
422 frequency bandwidths were used. Per session, there was only one spatial frequency bandwidth used to obtain
423 the characteristics of the adaptive procedure. To compare the different spatial frequency bandwidths all trials with
424 an orientation difference between 40° and 50° were included and averaged over all sessions. The *spatial*
425 *frequency discrimination task* followed a similar training regime. After the animals performed sufficient in the
426 pretraining, they were trained to discriminate between to motion clouds of different spatial frequencies. Over the
427 course of pre-training, the animals showed a stable discrimination between 0.04 and 0.16 cpd. after which
428 different orientation bandwidths were introduced. The different orientation bandwidths were used within a
429 session, because no adaptive staircase procedure was used in these experiments.

430 **Data analysis:** Two-photon imaging data were motion corrected and individual neurons were isolated with the
431 Suite2P package using model-based background subtraction[60]. The algorithm was used to perform rigid motion
432 correction on the image stack, identify neurons, extract their fluorescence and correct for neuropil contamination.
433 $\Delta F/F_0$ traces were produced using the method of Jia et al.[61], skipping the final filtering step. We then computed
434 the median fluorescence during the 5 s stimulus window for each stimulus presentation and subtracted the
435 median fluorescence during the preceding 1 s baseline. To determine if the response a given neuron to a visual
436 stimulus was significantly above baseline we computed the AUC for each stimulus against the baseline and
437 compared its value against a shuffle control, where stimulus and baseline labels were shuffled for each neuron.
438 This was repeated 100 times to create a distribution of shuffled AUC values for each neuron. A neuron was then
439 deemed significantly responsive to a given stimulus if the probability of obtaining the actual AUC from the

shuffled AUC distribution was less than 0.004 (0.05 / 12 to correct for multiple comparison bias). The mean number of responsive cells was normalized for each recording session by the number of neurons that responded to the lowest respective bandwidth. Statistical comparison of the different conditions was done in custom written MATLAB codes, comparing the number of responsive neurons over all recordings and mice. A Kruskal Wallis test was initially performed on all comparisons. For cases with paired comparisons (across experimental sessions), the nonparametric Wilcoxon signed rank test was subsequently performed to calculate significant differences between all compared pairs. For cases with non-paired comparisons (across pooled sessions, e.g. for all neurons), the nonparametric Wilcoxon rank sum test was used. To correct for multiple comparison bias, we performed Bonferroni correction. Plots were generated with the raincloud tool[62] and arranged in BioRender.com.

Acknowledgements

We would like to thank Laurent Perinet, Hugo Ladret, Ivo Vanzetta and Frédéric Chavanne for helpful insights on the motion cloud stimuli and coherent discussions on the project and manuscript; Madgalena Robacha for assistance with the mouse preparation and imaging and Gerion Nabbefeld for assistance with intrinsic imaging and the 2-photon setup. This work was supported by the Deutsche Forschungsgemeinschaft (DFG, German Research Foundation) - 368482240/GRK2416 and 430156848/SPP2205 and the Helmholtz association (VH-NG-1611).

Author contributions

B.M.K., C.W. and E.B., conceived and planned the experiments. E.B. designed the 2-Photon tasks, collected the neural data and performed the analysis with input from B.M.K and S.M. C.W. and J.L. designed the 2AFC task, collected the behavioral data and performed the analysis. E.B. wrote the initial draft and generated the figures with input from B.M.K and S.M. The manuscript was revised and completed by B.M.K and S.M. All authors read and approved the final manuscript. Correspondence should be directed to Björn Kampa, kampa@brain.rwth-aachen.de and Simon Musall, musall@bio2.rwth-aachen.de.

References

1. Simoncelli, E. P. & Olshausen, B. A. Natural Image Statistics and Neural Representation. *Annual Review of Neuroscience* **24**, 1193–1216 (2001).
2. Olshausen, B. & Field, D. Sparse coding of sensory inputs. *Current Opinion in Neurobiology* **14**, 481–487 (2004).
3. Bell, A. J. & Sejnowski, T. J. The "independent components" of natural scenes are edge filters. *Vision Research* **37**, 3327–3338 (1997).
4. van Hateren, J. H. & van der Schaaf, A. Independent component filters of natural images compared with simple cells in primary visual cortex. *Proceedings of the Royal Society of London. Series B: Biological Sciences* **265**, 359–366 (1998).
5. Hubel, D. H. & Wiesel, T. N. Receptive fields of single neurones in the cat's striate cortex. *J Physiol* **148**, 574–591 (1959).
6. Niell, C. M. & Stryker, M. P. Highly Selective Receptive Fields in Mouse Visual Cortex. *Journal of Neuroscience* **28**, 7520–7536 (2008).
7. Priebe, N. J. Mechanisms of Orientation Selectivity in the Primary Visual Cortex. *Annu. Rev. Vis. Sci.* **2**, 85–107 (2016).
8. Felsen, G., Touryan, J., Han, F. & Dan, Y. Cortical Sensitivity to Visual Features in Natural Scenes. *PLOS Biology* **3**, e342 (2005).
9. Schwartz, O. & Simoncelli, E. P. Natural signal statistics and sensory gain control. *Nat Neurosci* **4**, 819–825 (2001).
10. Girshick, A. R., Landy, M. S. & Simoncelli, E. P. Cardinal rules: visual orientation perception reflects knowledge of environmental statistics. *Nat Neurosci* **14**, 926–932 (2011).
11. Barlow, H. B. The coding of sensory messages. *Current problems in animal behavior* 331–360 (1961).
12. Stringer, C., Pachitariu, M., Steinmetz, N., Carandini, M. & Harris, K. D. High-dimensional geometry of population responses in visual cortex. *Nature* **571**, 361–365 (2019).
13. Walker, E. Y. *et al.* Inception loops discover what excites neurons most using deep predictive models | Nature Neuroscience. *Nature Neuroscience* **22**, 2060–2065 (2019).
14. Kayser, C., Körding, K. P. & König, P. Processing of complex stimuli and natural scenes in the visual cortex. *Current Opinion in Neurobiology* **14**, 468–473 (2004).
15. Stansbury, D. E., Naselaris, T. & Gallant, J. L. Natural Scene Statistics Account for the Representation of Scene Categories in Human Visual Cortex. *Neuron* **79**, 1025–1034 (2013).
16. Antolík, J., Hofer, S. B., Bednar, J. A. & Mrsic-Flogel, T. D. Model Constrained by Visual Hierarchy Improves Prediction of Neural Responses to Natural Scenes. *PLOS Computational Biology* **12**, e1004927 (2016).
17. Felsen, G. & Dan, Y. A natural approach to studying vision. *Nat Neurosci* **8**, 1643–1646 (2005).
18. Rust, N. C. & Movshon, J. A. In praise of artifice. *Nat Neurosci* **8**, 1647–1650 (2005).
19. Benda, J., Gollisch, T., Machens, C. K. & Herz, A. V. From response to stimulus: adaptive sampling in sensory physiology. *Current Opinion in Neurobiology* **17**, 430–436 (2007).
20. Leon, P. S., Vanzetta, I., Masson, G. S. & Perrinet, L. U. Motion clouds: model-based stimulus synthesis of natural-like random textures for the study of motion perception. *Journal of Neurophysiology* **107**, 3217–3226 (2012).
21. Simoncini, C., Perrinet, L. U., Montagnini, A., Mamassian, P. & Masson, G. S. More is not always better: adaptive gain control explains dissociation between perception and action. *Nature Neuroscience* **15**, 1596–1603 (2012).
22. Carandini, M. & Heeger, D. J. Normalization as a canonical neural computation. *Nat Rev Neurosci* **13**, 51–62 (2012).

23. Ferguson, K. A. & Cardin, J. A. Mechanisms underlying gain modulation in the cortex. *Nat Rev Neurosci* **21**, 80–92 (2020).
24. Bonin, V., Histed, M. H., Yurgenson, S. & Reid, R. C. Local Diversity and Fine-Scale Organization of Receptive Fields in Mouse Visual Cortex. *J. Neurosci.* **31**, 18506–18521 (2011).
25. Froudarakis, E. *et al.* Population code in mouse V1 facilitates readout of natural scenes through increased sparseness. *Nat Neurosci* **17**, 851–857 (2014).
26. Kampa, B., Roth, M., Göbel, W. & Helmchen, F. Representation of visual scenes by local neuronal populations in layer 2/3 of mouse visual cortex. *Frontiers in Neural Circuits* **5**, (2011).
27. Niell, C. M. Cell Types, Circuits, and Receptive Fields in the Mouse Visual Cortex. *Annu. Rev. Neurosci.* **38**, 413–431 (2015).
28. Roth, M. M., Helmchen, F. & Kampa, B. M. Distinct Functional Properties of Primary and Posteromedial Visual Area of Mouse Neocortex. *Journal of Neuroscience* **32**, 9716–9726 (2012).
29. Ganguli, D. & Simoncelli, E. Implicit encoding of prior probabilities in optimal neural populations. in *Advances in Neural Information Processing Systems* vol. 23 (Curran Associates, Inc., 2010).
30. Andermann, M. L., Kerlin, A. M., Roumis, D. K., Glickfeld, L. L. & Reid, R. C. Functional Specialization of Mouse Higher Visual Cortical Areas. *Neuron* **72**, 1025–1039 (2011).
31. Marshel, J. H., Garrett, M. E., Nauhaus, I. & Callaway, E. M. Functional Specialization of Seven Mouse Visual Cortical Areas. *Neuron* **72**, 1040–1054 (2011).
32. Muir, D. R., Molina-Luna, P., Roth, M. M., Helmchen, F. & Kampa, B. M. Specific excitatory connectivity for feature integration in mouse primary visual cortex. *PLOS Computational Biology* **13**, e1005888 (2017).
33. Muir, D. R., Roth, M. M., Helmchen, F. & Kampa, B. M. Model-based analysis of pattern motion processing in mouse primary visual cortex. *Frontiers in Neural Circuits* **9**, (2015).
34. Palagina, G., Meyer, J. F. & Smirnakis, S. M. Complex Visual Motion Representation in Mouse Area V1. *J. Neurosci.* **37**, 164–183 (2017).
35. Barbera, D., Priebe, N. J. & Glickfeld, L. L. Feedforward mechanisms of cross-orientation interactions in mouse V1. *Neuron* **110**, 297-311.e4 (2022).
36. Ruderman, D. & Bialek, W. Statistics of Natural Images: Scaling in the Woods. in *Advances in Neural Information Processing Systems* vol. 6 (Morgan-Kaufmann, 1993).
37. Wiesbrock, C., Musall, S. & Kampa, B. M. A flexible Python-based touchscreen chamber for operant conditioning reveals improved visual perception of cardinal orientations in mice. *Front Cell Neurosci* **16**, 866109 (2022).
38. Smith, A. T. & Edgar, G. K. The influence of spatial frequency on perceived temporal frequency and perceived speed. *Vision Research* **30**, 1467–1474 (1990).
39. Diener, H. C., Wist, E. R., Dichgans, J. & Brandt, Th. The spatial frequency effect on perceived velocity. *Vision Research* **16**, 169-IN7 (1976).
40. Jogan, M. & Stocker, A. A. Signal Integration in Human Visual Speed Perception. *J. Neurosci.* **35**, 9381–9390 (2015).
41. Nurminen, L., Merlin, S., Bijanzadeh, M., Federer, F. & Angelucci, A. Top-down feedback controls spatial summation and response amplitude in primate visual cortex. *Nat Commun* **9**, 2281 (2018).
42. Vangeneugden, J. *et al.* Activity in Lateral Visual Areas Contributes to Surround Suppression in Awake Mouse V1. *Current Biology* **29**, 4268-4275.e7 (2019).

43. Keller, A. J., Roth, M. M. & Scanziani, M. Feedback generates a second receptive field in neurons of the visual cortex. *Nature* **582**, 545–549 (2020).
44. Nassi, J. J., Lomber, S. G. & Born, R. T. Corticocortical Feedback Contributes to Surround Suppression in V1 of the Alert Primate. *J Neurosci* **33**, 8504–8517 (2013).
45. Blakemore, C. & Tobin, E. A. Lateral inhibition between orientation detectors in the cat's visual cortex. *Exp Brain Res* **15**, 439–440 (1972).
46. Van den Bergh, G., Zhang, B., Arckens, L. & Chino, Y. M. Receptive-field properties of V1 and V2 neurons in mice and macaque monkeys. *J Comp Neurol* **518**, 2051–2070 (2010).
47. Kirchberger, L. *et al.* The essential role of recurrent processing for figure-ground perception in mice. *Science Advances* **7**, eabe1833 (2021).
48. Keller, G. B. & Mrsic-Flogel, T. D. Predictive Processing: A Canonical Cortical Computation. *Neuron* **100**, 424–435 (2018).
49. Rao, R. P. N. & Ballard, D. H. Predictive coding in the visual cortex: a functional interpretation of some extra-classical receptive-field effects. *Nat Neurosci* **2**, 79–87 (1999).
50. Bastos, A. M. *et al.* Canonical microcircuits for predictive coding. *Neuron* **76**, 695–711 (2012).
51. Priebe, N. J. & Ferster, D. Mechanisms underlying cross-orientation suppression in cat visual cortex. *Nat Neurosci* **9**, 552–561 (2006).
52. Busse, L., Wade, A. R. & Carandini, M. Representation of Concurrent Stimuli by Population Activity in Visual Cortex. *Neuron* **64**, 931–942 (2009).
53. DeAngelis, G. C., Robson, J. G., Ohzawa, I. & Freeman, R. D. Organization of suppression in receptive fields of neurons in cat visual cortex. *Journal of Neurophysiology* **68**, 144–163 (1992).
54. Freeman, T. C. B., Durand, S., Kiper, D. C. & Carandini, M. Suppression without Inhibition in Visual Cortex. *Neuron* **35**, 759–771 (2002).
55. Ringach, D. L. The geometry of masking in neural populations. *Nat Commun* **10**, 4879 (2019).
56. Guan, S.-C., Zhang, S.-H., Zhang, Y.-C., Tang, S.-M. & Yu, C. Plaid Detectors in Macaque V1 Revealed by Two-Photon Calcium Imaging. *Current Biology* **30**, 934-940.e3 (2020).
57. Juavinett, A. L. & Callaway, E. M. Pattern and Component Motion Responses in Mouse Visual Cortical Areas. *Current Biology* **25**, 1759–1764 (2015).
58. Han, X., Vermaercke, B. & Bonin, V. Diversity of spatiotemporal coding reveals specialized visual processing streams in the mouse cortex | Nature Communications. *Nature Communications* **13**, 3249 (2022).
59. Adesnik, H., Bruns, W., Taniguchi, H., Huang, Z. J. & Scanziani, M. A neural circuit for spatial summation in visual cortex. *Nature* **490**, 226–231 (2012).
60. Pologruto, T. A., Sabatini, B. L. & Svoboda, K. ScanImage: Flexible software for operating laser scanning microscopes. *BioMedical Engineering OnLine* **2**, 13 (2003).
61. Jia, H., Rochefort, N. L., Chen, X. & Konnerth, A. In vivo two-photon imaging of sensory-evoked dendritic calcium signals in cortical neurons. *Nat Protoc* **6**, 28–35 (2011).
62. Allen, M., Poggiali, D., Whitaker, K., Marshall, T. R. & Kievit, R. A. Raincloud plots: a multi-platform tool for robust data visualization. *Wellcome Open Res* **4**, 63 (2019).

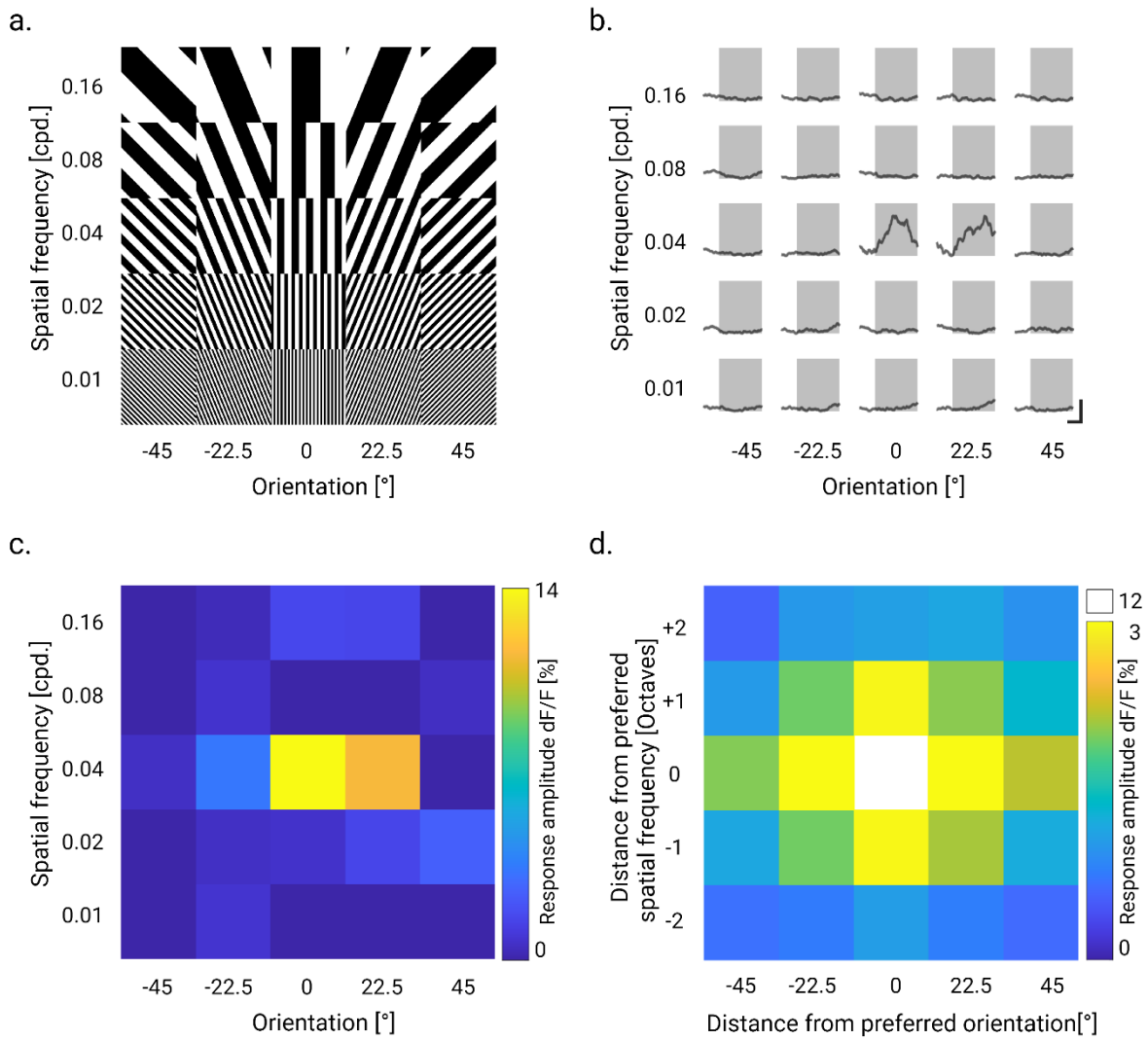

Figure S1. V1 tuning specificity to orientation and spatial frequency of grating stimuli
(**a**) Overview of 25 combinations of visual grating stimuli, consisting of 5 different orientations (-45°; -22.5°; 0°; 22.5°; 45°) and spatial frequencies (0.01cpd; 0.02cpd; 0.04cpd; 0.08cpd; 0.16cpd). All stimuli were presented as pseudorandom sequences to 3 awake mice in 6 sessions. (**b**) Mean response traces of an example V1 neuron for each stimulus combination. Shaded area is the stimulus duration. (Scale bar: 1s, 20% dF/F). (**c**) Average response strength to each stimulus combination for the neuron shown in panel b. (n = XX presentations per stimulus). Clearly visible is a narrow orientation and spatial frequency tuning. (**d**) Averaged tuning specificity for all responsive V1 neurons (n = 971 cells). For each neuron, the response matrix was shifted so that the peak orientation and spatial frequency response was in the center. X- and Y-axes therefore show the distance from the preferred orientation and spatial frequency, measuring thus the width of the population orientation and spatial frequency tuning within the presented stimulus range. Paired Wilcoxon sing rank test of the full-width half maximum (FWHM) of a gaussian fit in the central x axis (for orientation) and y axis (for spatial frequency) showed a small but significant difference among the two tuning widths $FWHM_{orientation}$ = 1.76 ± 0.04 bins, $FWHM_{spatial\ frequency}$ = 1.67 ± 0.04 bins (Wilcoxon sign rank test, p value = 1.91e-38). This suggests that V1 neurons were slightly less selective for grating orientations. Importantly, this is the opposite of what would have been expected if the selective increase in neural responses to broad orientation bandwidth would have been caused by additional recruitment of V1 subpopulations with very narrow orientation tuning.

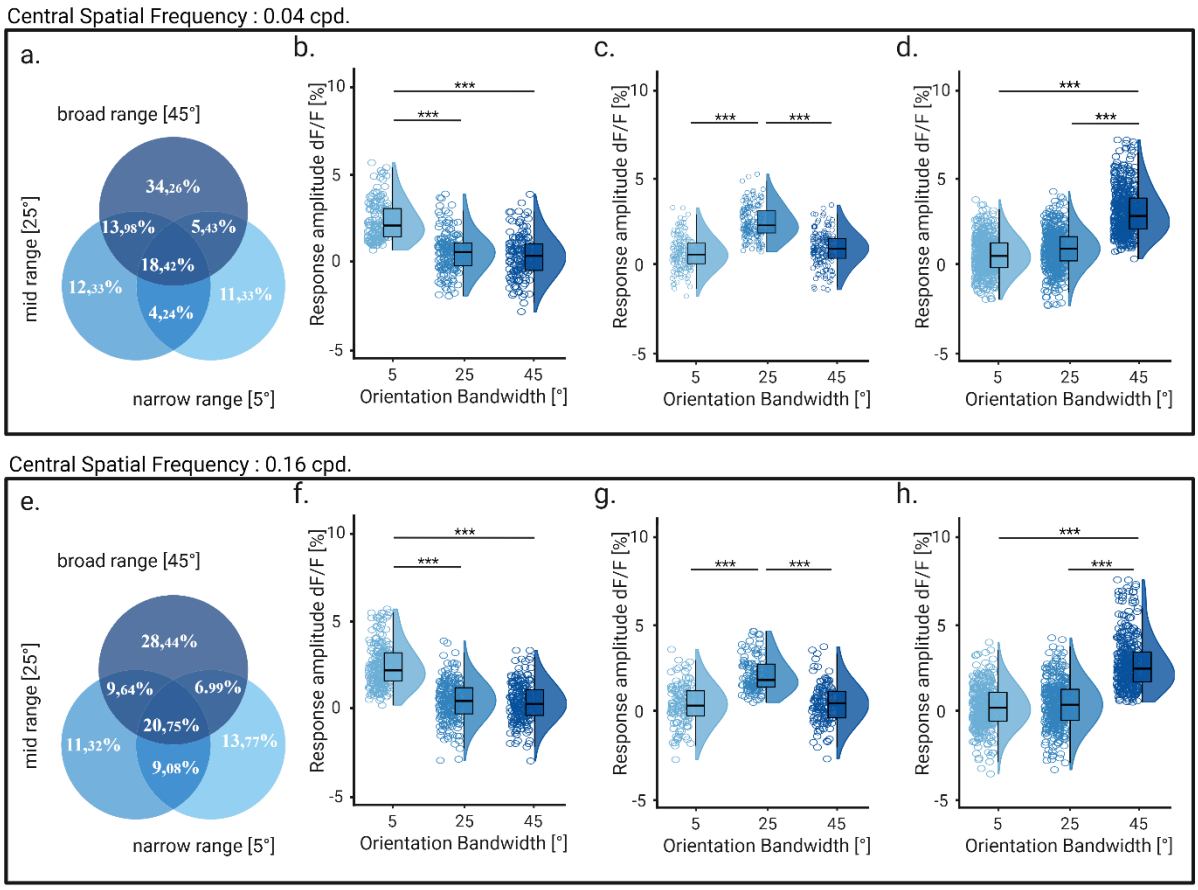

Figure S2. V1 neurons show orientation bandwidth tuning, across different central spatial frequencies. (**a**) Venn diagram shows the distribution of neurons that significantly responded to a single or multiple orientation bandwidths. Shown are percentages for all responsive neurons (1509 out of 4892 neurons in total). (**b**) Difference between mean response amplitude versus baseline for each orientation bandwidth. Shown are all neurons that selectively responded to the narrow-range bandwidth. n = 171 neurons. (**c**) Same as in panel b but only for neurons that selectively responded to the mid-range bandwidth. n = 186 neurons. (**d**) Same as in panel b but only for neurons that selectively responded to the broad-range bandwidth. n = 517 neurons. (**e-h**) Same as in panels a-d but for the central spatial frequency of 0.16 cpd. Strong tuning to different bandwidths and increased responses to broadband orientation stimuli were similarly observed as with the central spatial frequency of 0.04 cpd. Respective cell numbers per respective plot: n = 1428 total out of 4829, n = 197 narrow band preferring, n = 162 mid band preferring, n = 407 broad band preferring. Stars in all panels show Bonferroni-corrected significance from a two-sided Wilcoxon signed rank test.

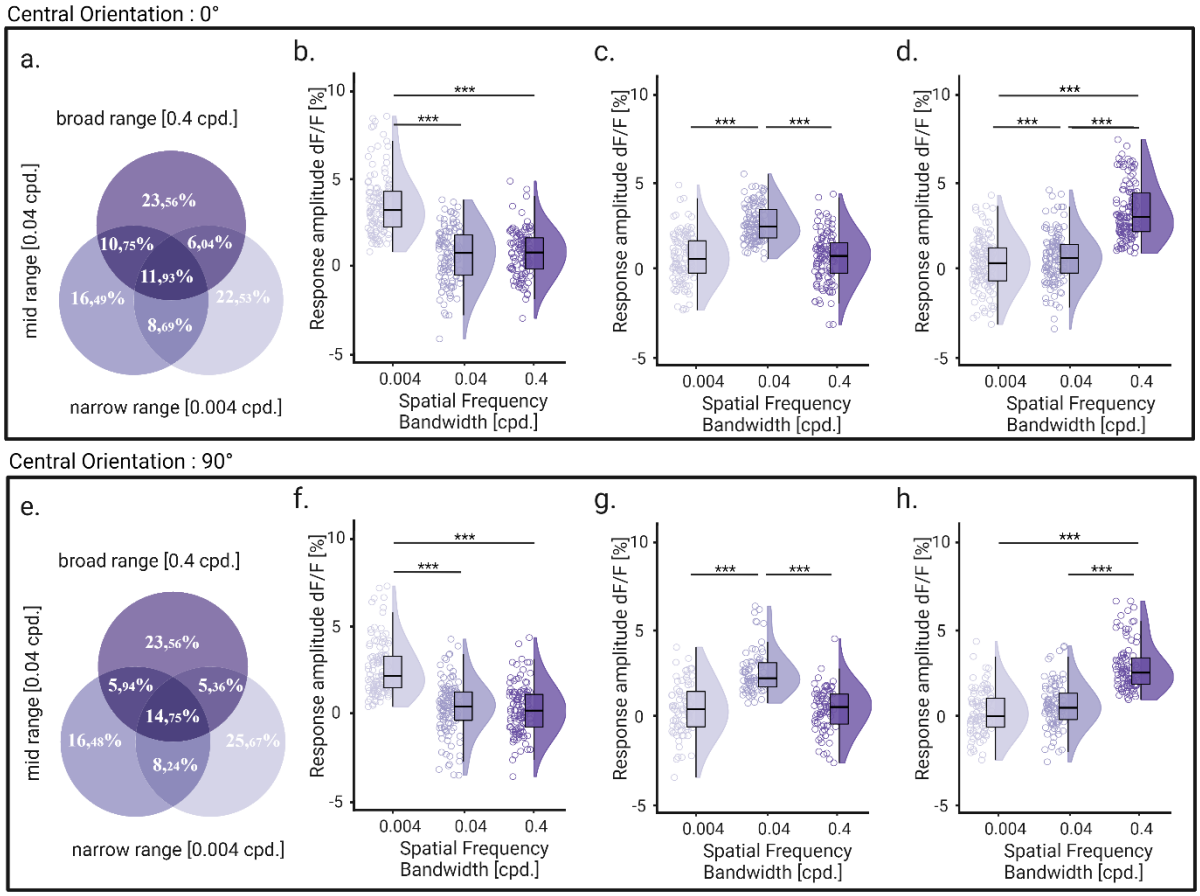

Figure S3. V1 neurons show orientation bandwidth tuning, spanning across different central orientations. (**a**) Venn diagram shows the distribution of neurons that significantly responded to a single or multiple spatial frequency bandwidths. Shown are percentages for all responsive neurons (679 out of 3185 neurons in total). (**b**) Difference between mean response amplitude versus baseline for each spatial frequency bandwidth. Shown are all neurons that selectively responded to the narrow-range bandwidth. n = 153 neurons. (**c**) Same as in panel b but only for neurons that selectively responded to the mid-range bandwidth. n = 112 neurons. (**d**) Same as in panel b but only for neurons that selectively responded to the broad-range bandwidth. n = 160 neurons. (**e-h**) Same as in panels a-d but for the central orientation of 90°. High specificity and very little overlap across the three spatial frequency bands was observed in both cases. Respective cell numbers per respective plot: n = 522, n = 134, n = 86, n = 123. Stars in all panels show Bonferroni-corrected significance from a two-sided Wilcoxon signed rank test.